

Copyright 2006 Society of Photo-Optical Instrumentation Engineers. This paper was published in “*Advances in Stellar Interferometry*”, *Proc. SPIE 6268, 2006* and is made available as an electronic reprint with permission of SPIE. One print or electronic copy may be made for personal use only. Systematic or multiple reproduction, distribution to multiple locations via electronic or other means, duplication of any material in this paper for a fee or for commercial purposes, or modification of the content of the paper are prohibited.

# Design and testing of an innovative delay line for the MROI

David F. Buscher, Roger C. Boysen, Roger Dace, Martin Fisher, Christopher A. Haniff,  
Eugene B. Seneta, Xiaowei Sun, Donald M. A. Wilson, John S. Young

Cavendish Laboratory, J. J. Thomson Avenue, Cambridge CB3 0HE, U.K.

## ABSTRACT

The delay lines currently under development for the MROI Interferometer will provide up to 380m of optical delay with only 3 reflections. We describe the novel aspects of the delay line design which include using the inside walls of the vacuum pipes as “rails”, active shear compensation, and replacing dragged cables with contactless power transfer and communication. We describe the results of tests of various of these design concepts, and progress on the design and construction of the prototype trolley.

**Keywords:** optical delay line, stellar interferometry

## 1. INTRODUCTION

The current generation of optical and infrared interferometers are beginning to show that interferometry can provide new and interesting results to a range of astrophysical questions. Nevertheless, there are a number of key performance criteria which must be addressed before interferometry will be thought of as a “mainstream” tool of astronomy. Chief amongst these is the ability to access a wide range of targets, especially extragalactic targets such as AGN. This implies that the magnitude limit of interferometers must be increased by several magnitudes from the current range of around 7th to 9th magnitude at near-infrared wavelengths to at least 13th or 14th magnitude in order to access reasonable samples of such objects.<sup>1</sup>

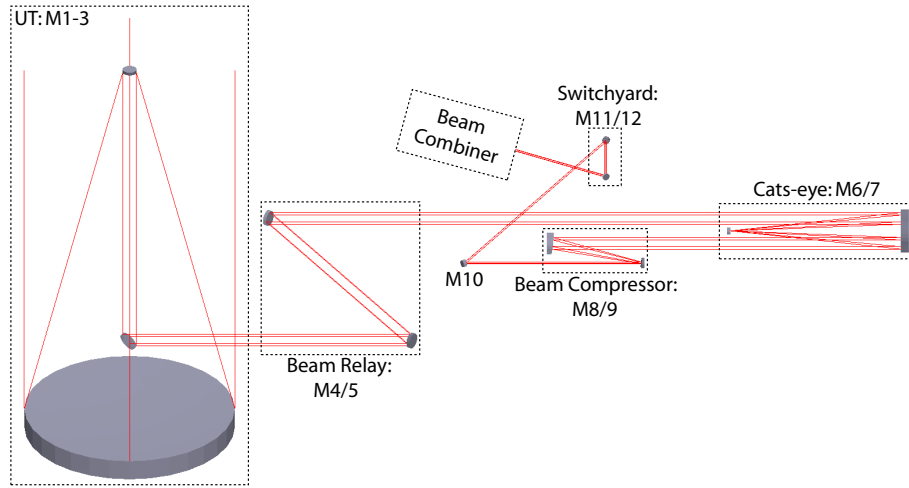
In order to achieve these increases in limiting magnitude, we need to improve the “interferometric throughput” of interferometers, that is, we need to reduce the often large instrumental losses of both stellar light flux and wavefront quality which degrade the interferometric signal-to-noise ratio (SNR). One key factor in achieving low losses is to reduce the number of reflections of the optical beam between the sky and the detector to the absolute minimum. Each reflection degrades the interferometric throughput in 3 ways: it reduces the photon throughput due to reflection losses, it introduces high-order wavefront aberrations due to mirror figure errors, and it degrades the low-order wavefront quality by adding an extra surface which needs to be aligned (in tip and tilt for flat mirrors as well as focus and other degrees of freedom for curved surfaces). Remembering that the fringe visibility losses scale approximately as the square of the RMS wavefront error and the interferometric SNR scales as the square of the fringe visibility, we can see that the most deleterious effects of adding extra reflections are to do with wavefront quality degradation.

Fig. 1 shows a schematic of the optical train of the MROI interferometer (Crech-Eakman *et al.*, these proceedings, paper 6268-70), which has been optimised for imaging of faint objects. The total number of reflections experienced by starlight between the sky and the entrance of the beam combiner instrument is 13, which compares favourably with other interferometers. For example, the comparable value in the VLTI is 22 reflections<sup>2</sup> and in the Keck Interferometer the starlight beam encounters 19 reflective elements *after* exiting the adaptive optics systems on the telescopes.<sup>3</sup>

An important factor in the MROI design is that only 3 reflections are required in order to achieve optical path compensation and this is achieved by using a single-stage optical delay-line. Most other interferometers with baselines greater than 100 m use multi-stage delay-lines in order to achieve the long delay strokes required to access different areas of the sky. An example of this is shown in Fig. 2 which shows the long delay line (LDL) portion of the pathlength compensation system for NPOI.<sup>4</sup> Like the Keck and CHARA path compensation systems, the NPOI system uses a two-stage system for delay compensation on long baselines: the LDL puts in different amounts of quasi-static delay and this is used in conjunction with a fast delay line (FDL) stage which

---

D.F.B.: E-mail: dfb@mrao.cam.ac.uk, Telephone: +44 (0)1223 337302



**Figure 1.** A schematic view of the optical train of the MROI, showing the reflective surfaces encountered by light going from a star to the entrance to a beam combiner. The light beam goes through only 13 reflections in this train (there are only 12 mirrors because the beam bounces off M6 twice)

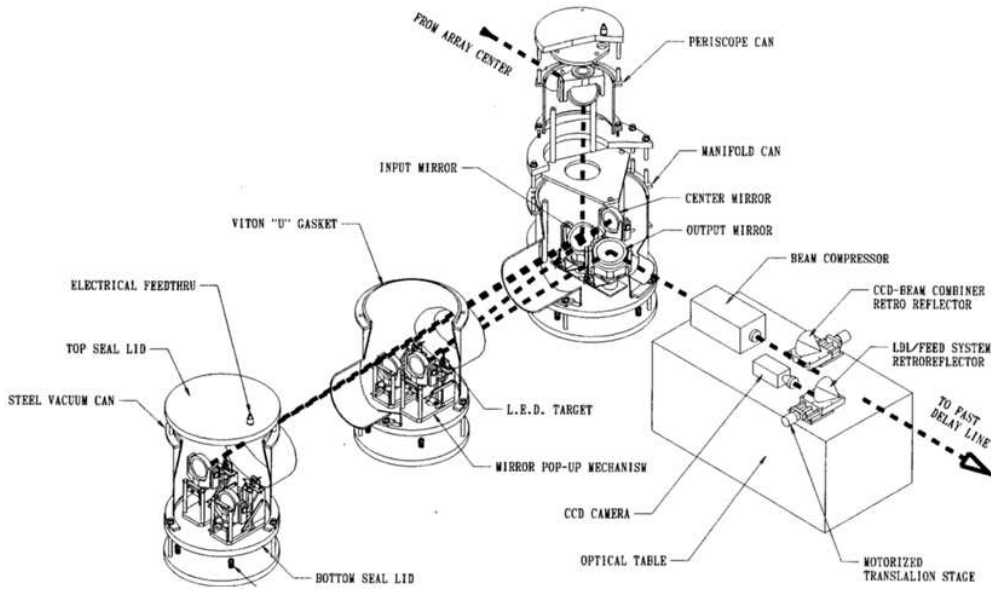


**Figure 2.** Diagram of the Long Delay Lines at NPOI (from Ref. 4)

tracks sidereal and atmospheric motions. As can be seen from the diagram, the NPOI LDLs add an extra 4 reflections (plus 2 reflections which “periscope” the beam) when compared with the FDLs alone. This level of increase in the number of reflections is not untypical for such multi-stage systems.

The MROI delay line design aims to do away with the extra reflections, and hence losses, associated with multi-stage delay lines, as part of an overall efficient design suitable for faint-object science. At the same time the single-stage system reduces system complexity and hence operational and maintenance overheads when compared with multi-stage systems. In order to achieve this goal, our design introduces a number of concepts not used before in interferometer delay lines. Here we describe the design of the delay line and the results of the testing we have performed on the innovative design concepts employed. We also report on the status of the delay line prototyping effort.

## 2. BACKGROUND AND REQUIREMENTS

The optical interferometry group in Cambridge designed and built the delay lines for the COAST interferometer which saw first fringes in 1991.<sup>5</sup> Since then the group has been developing concepts for next-generation interferometers, including the associated high-throughput delay lines. In January 2005, the COAST group signed a contract with New Mexico Tech (NMT) for Cambridge to design and prototype the delay lines for the MROI, and to deliver the first production delay line trolley. This work is also partly funded by a Rolling Grant from the UK's Particle Physics and Astronomy Research Council (PPARC).

The top-level functional requirements for the MROI delay line can be summarised as follows:

**Stroke:** Compensation for up to 380 m of optical delay. Rationale: this will allow the equalisation of the optical path delay (OPD) between any set of telescopes situated on a “Y” array with arm lengths of 200 m, for all stars above 30° in elevation.

**Slew speed:** Less than 30 seconds to introduce a 30 m change in OPD, and less than 5 minutes to traverse the entire OPD range. Rationale: 30 m of OPD change is required to switch between two stars separated by 5° on the sky on a 350 m baseline. The goal for the interferometer is to be able to switch between two such stars and be taking data with a total overhead of less than 60 seconds.

**Sidereal tracking and jitter:** Sidereal tracking of up to 30 mm/s OPD fringe rate with a jitter of less than 15 nm rms as measured over any 10 ms interval, a jitter of less than 41 nm rms over any 35 ms interval, and a jitter of less than 55 nm rms over any 50 ms interval. Rationale: the tracking velocity given corresponds to the maximum sidereal rate for a 400m baseline. The jitter values given correspond to a  $\lambda/40$  rms OPD jitter over a  $2t_0$  integration at wavelengths of 600 nm, 1650 nm and 2200 nm respectively, when  $t_0$  at 500 nm wavelength is 4 ms.

**Dynamic tracking of atmospheric fluctuations:** Accepts commands from an external fringe tracker with a step response time of less than 30ms for step sizes of up to 10 microns. Goal: step response time of less than 2ms for step sizes of up to 0.5 microns. Rationale: The requirement supports low-bandwidth coherencing on faint stars while the goal supports a high-bandwidth hardware cophasing mode on bright stars.

**Clear aperture:** 125mm diameter. Rationale: the collimated beam diameter at the telescope is 95mm and an extra 30% must be allowed for diffraction and misalignment.

**Static wavefront quality:** 60nm rms across the clear aperture, including focus errors. Rationale: this requirement derives from the overall interferometer wavefront quality error budget.

**Dispersion:** Less than 0.175 radians of differential optical phase change across any bandpass (after subtracting the linear component of phase change with wavenumber) with a fractional bandwidth of 5% anywhere within the J, H and K astronomical photometric bands and across any bandpass with a fractional bandwidth of 0.5% anywhere within the astronomical R and I bands. Rationale: this requirement derives from the fringe curvature part of the spectral dispersion component of the interferometer visibility loss error budget.

**Polarisation:** Less than 1% di-attenuation for light of wavelengths between 600nm and 2400nm. Rationale: this requirement derives from the overall interferometer system goal to maintain high polarisation fidelity.

**Pupil shear:** Less than 1mm rms variations in the position of the centre of the starlight exit beam. Rationale: this requirement derives from the overall interferometer visibility loss error budget: a 1mm shear results in a 1% fringe visibility loss.

**Optical throughput:** Less than 15% throughput loss for light at wavelengths between 600 and 2400nm. Rationale: This is derived from the system throughput error budget.

### 3. DESIGN APPROACH

The key design approach we have adopted is to aim for a scalable design, by which we mean we are aiming for a design where the cost of the delay line scales approximately linearly with the maximum delay, with a coefficient of proportionality which is as low as possible. If by introducing some extra one-off costs, for example by making the retro-reflector more expensive, we can reduce this scaling coefficient, then the overall cost for achieving a long delay can be minimised.

The dominant cost for a long-stroke delay line is associated with the combined requirements for operation in a vacuum (to meet dispersion requirements) and for the retro-reflector to run on precise rails (to meet beam shear and OPD stability requirements). Typically the solution adopted is to fix polished steel rails inside vacuum pipes, but this is costly, particularly in terms of the time taken to install the rails inside the pipes and align them to the required precision. In the MROI design, we have taken a radical approach and removed the rails altogether. Instead, the inner walls of the vacuum pipes act as the guides for the trolley. The thick-walled (0.5 inch) pipes also act as their own mechanical platform, eliminating the need to mount the delay lines on optical benches.

By thus reducing the installation costs and by using commercial extruded aluminium pipe, we have substantially reduced the total cost per metre of the delay line compared with existing solutions. Two innovations make this possible. Firstly the optical retro-reflector has an active control loop which maintains the return light beam position (shear) in spite of small errors in pipe straightness, and secondly the separate carriage with resilient wheels allows smooth motion in spite of roughness or unevenness of the pipe surface. We describe our delay line concept in more detail below.

### 4. CONCEPT DESCRIPTION

Optical path compensation is achieved by bouncing the starlight off a moving retro-reflector (Cat's-eye) inside a vacuum pipe. The components of the complete path compensation system (for one telescope unless stated) are as follows:

1. A "trolley" consisting of a cylindrical "carriage" supporting and enclosing the cylindrical Cat's-eye.
2. 200 m of vacuum pipe to support and guide the trolley, supported on flexure legs to accommodate thermal expansion.
3. A laser metrology system to measure the position of the Cat's-eye by bouncing a laser beam off it. The laser is fed into and out of the "near" end of the vacuum pipe, in the Beam Combining Area (BCA). Each laser head is used for up to six trolleys.
4. A shear sensor in the BCA, which uses a small fraction of the metrology light to sense the position of the metrology beam and hence the shear of the science beam.
5. An inductive power supply to deliver electrical power to the trolley, via a wire lying in the bottom of the vacuum pipe. The wire slides through a long thin transformer on the trolley which inductively couples high-frequency (20kHz) electrical power from the wire to the trolley.
6. A distributed control system involving the following computers:
  - A "workstation" PC (shared between all trolleys) to act as a supervisor, and provide a user interface for testing the delay line and interrogating delay line telemetry.
  - A VME-bus CPU (shared between all trolleys) to read the metrology signal and hence control the Cat's-eye.
  - A low-power PC104 single-board micro on each trolley, to control on-board functions with undemanding timing requirements, and to send telemetry to the workstation.
  - Two separate radio-frequency (RF) links between the trolley and the external control system:
    - A low-latency 900 MHz link used to close the Optical Path Delay (OPD) loop in "Tracking" mode.

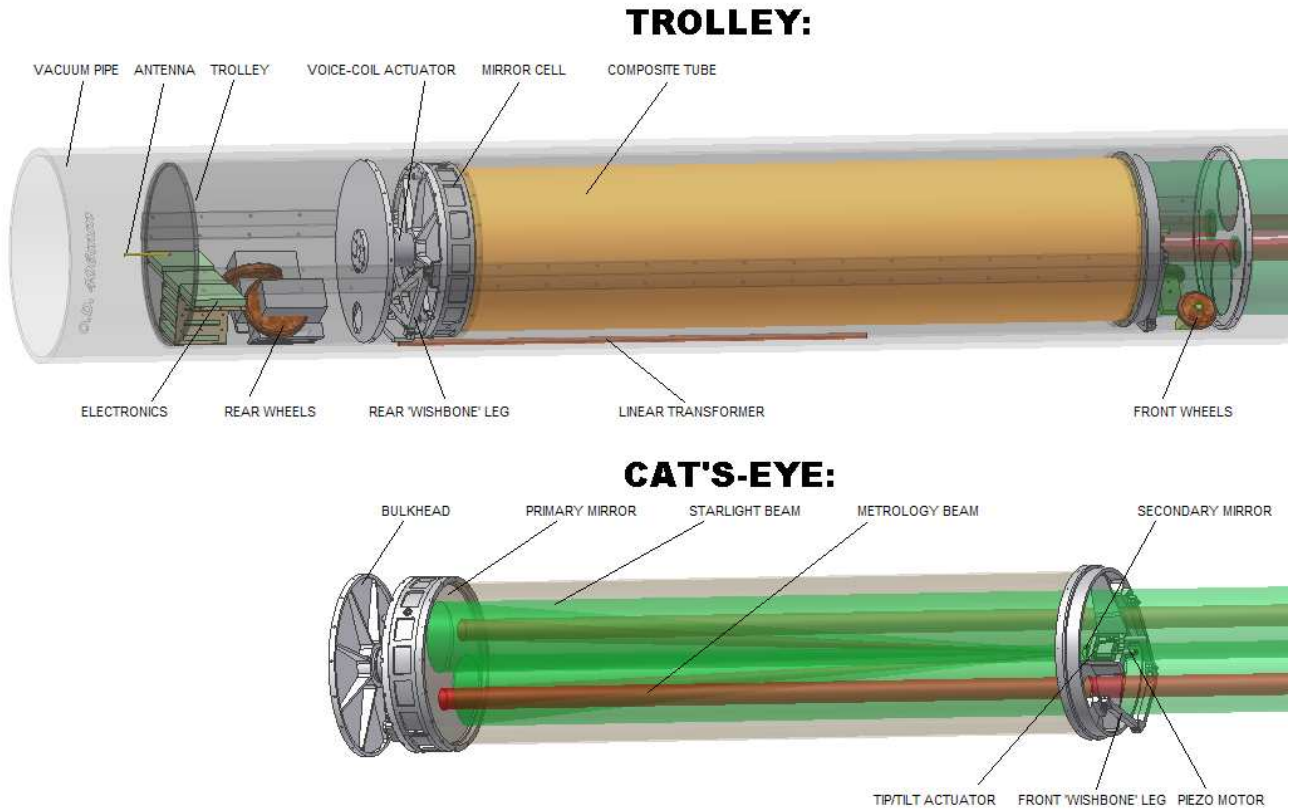


**Figure 3.** Concept diagram for the prototype delay line trolley, showing the physical locations and space envelope of the active elements. Components referred to in the text are labelled. The top part of the diagram shows the complete trolley (comprising the Cat’s-eye and carriage) inside the vacuum pipe, and the lower part is an expanded view of the Cat’s-eye. The diameter of the carriage tube is approximately 14 inches, and the approximate wheelbase of the carriage is 1.8 m.

- A standard 2.4 GHz wireless Ethernet link used for communication between the on-board micro and external control computers.
- 7. A “datum” switch, to act as a fixed fiducial point on the pipe from which to reference the laser metrology measurement.
- 8. Speed limit switches, to force the trolley to slow down when it approaches either end of the pipe.

Fig. 3 shows a diagram of the trolley concept. The details of the subsystems involved are described in the subsections below.

#### 4.1. The Cat’s-eye

The Cat’s-eye has two major components, a large parabolic primary mirror, and a small flat secondary mirror at its focus. A parallel beam of light striking the primary mirror is brought to a focus on the secondary mirror, reflected back to the primary mirror, and returned parallel to its original direction.

The secondary mirror is attached to a piezo tip/tilt actuator. Tilting this mirror changes the lateral position (shear) of the starlight beam exiting the Cat’s-eye while maintaining the same exit beam direction. As the trolley moves along a pipe which is not perfectly straight, the lateral position of the Cat’s-eye will fluctuate, and in a Cat’s-eye with a fixed secondary this would cause the beam shear of the output beam to fluctuate. In the MROI design, the tilting secondary is used inside a low-bandwidth feedback loop (described below) to reduce these

fluctuations in the beam shear to less than  $\pm 1\text{mm}$ . This active shear control allows the trolley to run inside commercial extruded pipes which are only straight to  $\pm 5\text{mm}$ .

The complete Cat's-eye assembly is mounted in the carriage on two "wishbone" legs so it is free to move axially. The legs have flexure pivots to avoid friction and stiction, and a voice-coil actuator and a position sensor are mounted between the back of the mirror cell and a bulkhead in the carriage.

## 4.2. The Carriage

The carriage is a cylinder which concentrically encloses the Cat's-eye. The carriage is supported and guided in the pipe by four wheels with polyurethane tyres. This four point contact keeps the carriage and consequently the Cat's-eye axially aligned with the pipe. The wheels are set at  $45^\circ$  to the vertical for equal constraint in the horizontal and vertical directions.

One rear wheel is driven by a brushless DC servo motor while the other one is actively steered by small angles to correct any rotation of the trolley in the pipe. The linear transformer of the inductive power supply system is mounted under the carriage, and the antennae for the two RF data links on the back plate. The on-board control micro, drive and steering motor controllers, controllers for the Cat's-eye actuators, and power supply electronics are mounted in the space between the bulkhead and the back plate of the carriage, where waste heat can easily be transferred by conduction to the carriage shell and so dissipated to the surrounding pipe.

## 4.3. The Control System

There are several servo loops involved in the operation of the trolley. These are shown conceptually in Fig. 4, which includes both the loops entirely contained on the trolley and those relying on signals from external components, transmitted to the trolley via the RF data links. The individual control loops are described in more detail below.

### 4.3.1. OPD Control

There are two main modes of operation for this loop. In either case the position of the Cat's-eye is measured by the laser metrology system, and the relative position of the Cat's-eye and the carriage is measured by an on-board sensor. However, the measurements are used in somewhat different ways in the two modes.

**Tracking** This is the most critical mode, used when recording science data. The OPD control loop is a two-stage loop very similar to that used successfully on the COAST delay lines. The two stages of the loop are:

**Cat's-eye** The Cat's-eye position is measured by the laser metrology system and compared at a 5kHz sample rate (by the VME CPU) with the current demanded position (interpolated from positions sent slightly in advance from the workstation). The resulting error signal is sent via the dedicated low latency ( $<50\mu\text{s}$ ) RF link to the trolley, where it is amplified and used directly to drive the Cat's-eye voice coil actuator.

**Carriage** The carriage drive motor is directly controlled by the relative position sensor to keep the carriage centred under the Cat's-eye so the "wishbone" legs are upright. This is important for best noise rejection. A demanded velocity term sent via the Ethernet RF link is added to reduce tracking error.

**Slewing** This mode is used for rapid re-positioning of the trolley. The Cat's-eye voice coil is driven directly by the relative position sensor to hold it fixed relative to the carriage. The drive motor can then be ramped up to full speed until the desired position is approached and then slowed before reverting to tracking mode.

### 4.3.2. Shear Control

This is an "always-on" low frequency loop closed via the Ethernet RF link and on-board micro. The shear sensor in the BCA uses a small fraction of the metrology laser light to measure any shear, and sends correction signals to the tip/tilt stage in the secondary mount on the Cat's-eye. A schematic of this control scheme is shown in Fig. 5. Only a low bandwidth is required, but this may be altered depending on the speed of travel.

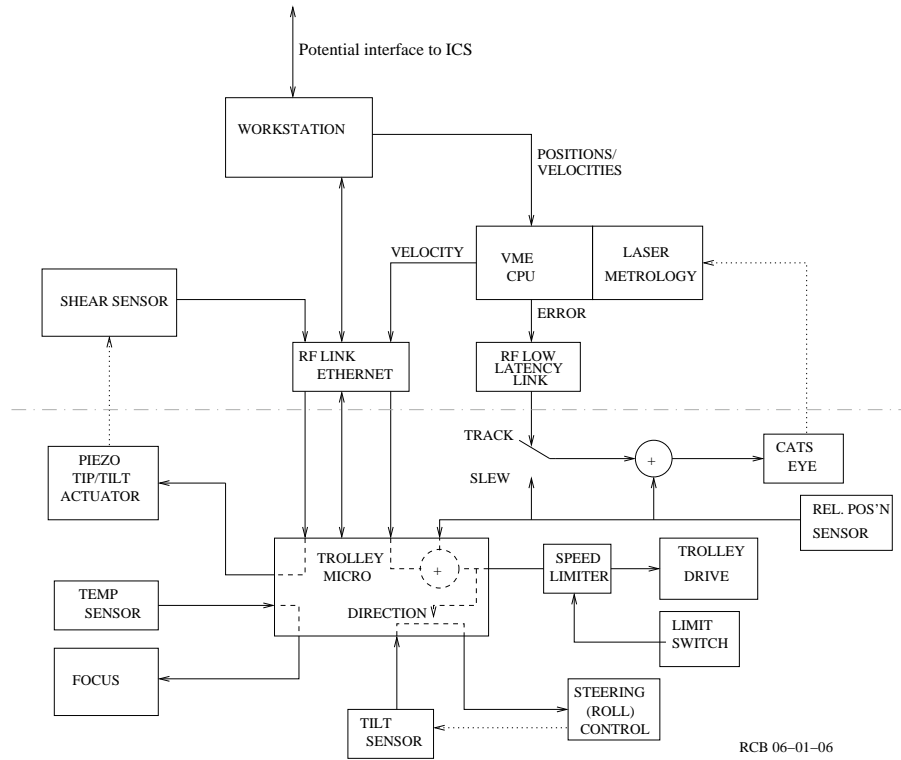


**Figure 4.** Overview of the control system for the prototype trolley, showing the origin of the signals used to control the active elements on the trolley. Components in the lower half of the diagram (except part of the speed limit switch) are physically located on the trolley. Each dotted line is drawn between an active element and a sensor whose output is *indirectly* affected by actuating the element. Dashed lines indicate connections made in software running on the on-board trolley micro. The “rel. pos’n sensor” measures the relative position of the Cat’s-eye with respect to the carriage.

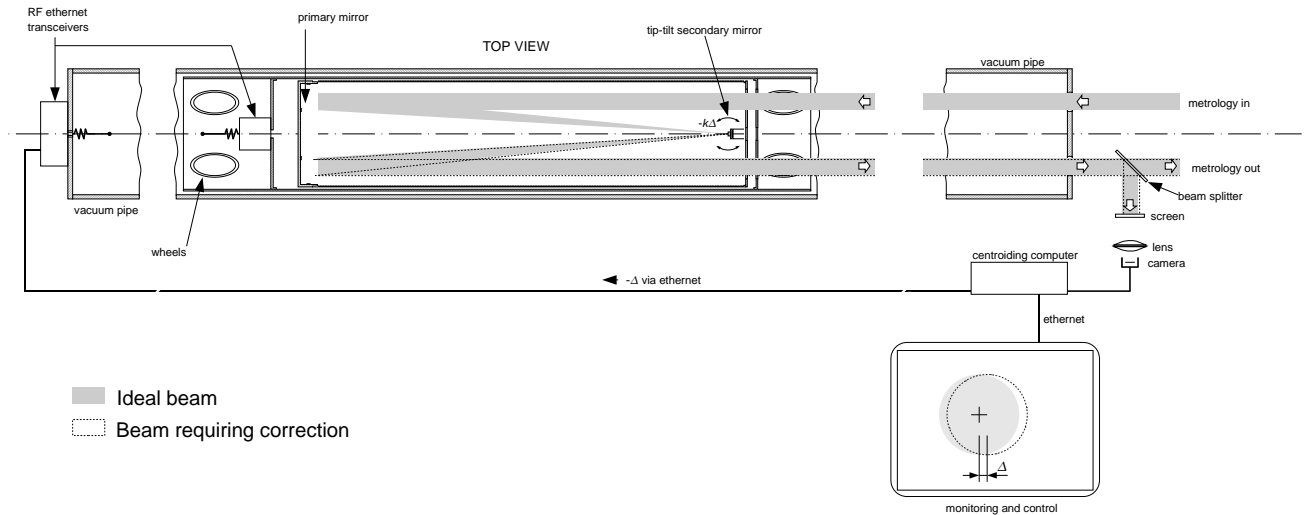


**Figure 5.** Schematic diagram of the servo loop for controlling the shear introduced by the Cat’s-eye as a result of imperfections in the straightness of the vacuum pipes.

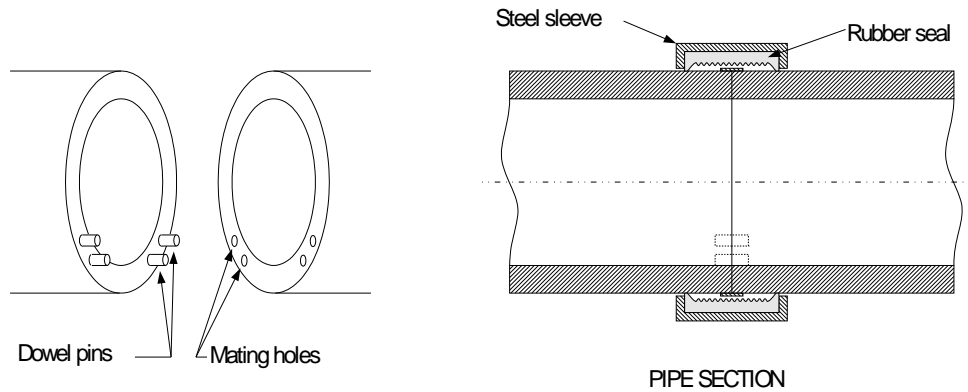


**Figure 6.** Sketch of the pipe coupling scheme, showing the arrangement of dowels which aligns the pipes at the points on the pipe circumference where the trolley wheels cross from one pipe to another. The resulting “steps” at the pipe joints were measured to be only a few tens of microns in height. The sketch also shows one of the candidate elastomeric vacuum seals for the pipe joints.

#### 4.3.3. Roll control

The trolley is “kinematically” constrained to move axially along the pipe, but is not constrained in rotation about the pipe axis. Some control of this “roll” degree of freedom is achieved by having the trolley centre of gravity below the centre line of the pipe. This is a robust control — it is then almost impossible to capsize a trolley — but it is not very accurate, and accuracy is needed for two reasons. Firstly the axes of the secondary tip/tilt stage have to be kept matched to the beam shear sensor, and secondly the trolley wheels have to follow relatively narrow tracks to cross the pipe joints where the surfaces are aligned. For accurate roll control an active trim system is included on the trolley. An electronic tilt sensor measures the roll angle of the trolley. This is digitised and read by the on-board micro, which controls a servo motor to adjust the tracking of the unpowered rear wheel to correct any error. This low frequency loop is entirely contained on the trolley.

#### 4.4. Pipes, coupling and supports

The vacuum enclosures are made of 12 foot lengths of extruded aluminium pipes 16 inches in diameter with 0.5 inch walls. The pipes are joined using elastomeric seals, as used for example on the NPOI delay lines.

In order to ensure that the wheels of the trolley do not experience a “bump” at each pipe joint, the pipe ends need to be precisely aligned with one another at the two points on the pipe circumference where the wheels run. This is achieved using dowels inserted in holes which are drilled in the pipe end using a precision jig. The pipe jointing scheme is shown in Fig. 6. Laboratory tests have shown that the resulting “steps” at the pipe junctions are less than  $\pm 30 \mu\text{m}$  in height.

The pipes deflect less than 0.1mm under their own weight and the weight of the trolley, so no extra support platforms, e.g. optical tables are required to give the necessary rigidity to the “rails”. The pipes do need to be supported in such a way as to accommodate seasonal thermal expansion and contraction: a 190m long stretch of pipes will expand by 14 cm when going between -10C and +20C. Consideration of various support schemes such as rigid mounting, rollers or sliding pads showed that either very large forces would have to be contained, or that quite large forces plus probable stick-slip motion would result. The only sensible method is to use flexure legs, and these have to be quite long – 1 m or so – to avoid excessive height changes at the “free” end of the pipes. However the flexibility at the joints of our proposed system of pipe jointing means that the pipe does not have to be forced to lie straight as it would with flanged joints if there was any build up of tolerances. Fig. 7 shows schematically the support scheme.

### 5. RISK REDUCTION EXPERIMENTS

Our design for the MROI delay line design has a relatively large number of features which have not been used before in delay line designs, and so it was decided to do a series of experiments and analyses to validate these

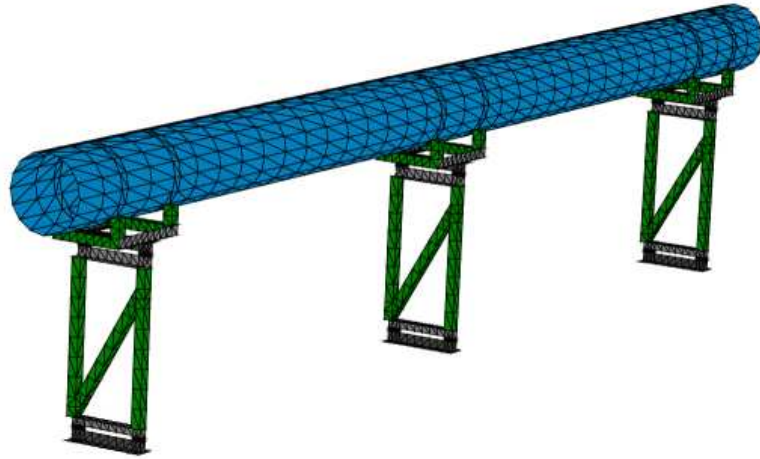


**Figure 7.** FEA analysis model of a run of 2 pipe lengths showing the pipes, flexure mountings and pipe cradles.

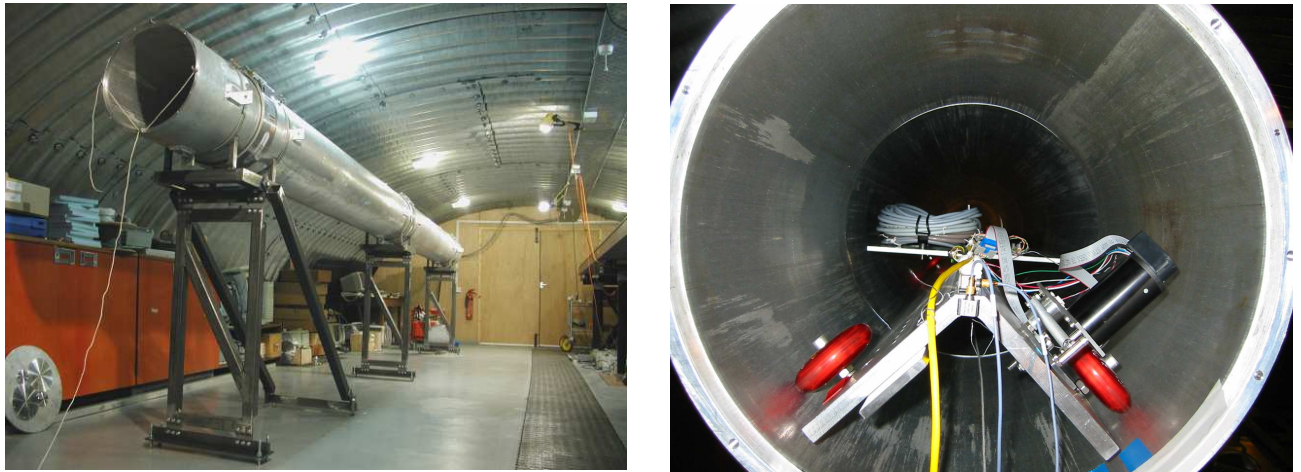


**Figure 8.** (Left) Photograph of the 7-metre-long test rig used for the risk reduction experiments. (Right) Photograph of the “embryo” trolley in the pipe test rig, showing the compliant wheels running at  $45^\circ$  to the vertical, the drive motor, and the cables for the accelerometers and other sensors.

concepts before proceeding with designing and constructing the prototype. The experiments employed a test rig consisting of a 7-metre-long run of 16-inch diameter pipes, as shown in the left-hand photo in Fig. 8. Tests of various aspects of the trolley concept were made using an “embryo” trolley consisting of a length of aluminium angle to which compliant wheels were attached, as shown in the right-hand photo in Fig. 8. Weights were added at various heights to effect changes in the height of the centre of gravity of the trolley for roll tests, and the trolley was motorised and outfitted with accelerometers in order to measure the level of vibration induced when running on the unfinished pipe surface. A test of the inductive power supply and RF communication was made by retrofitting one of the COAST trolleys with prototypes of these “contactless” technologies.

A large number of tests were made of most of the innovative aspects of our design, and we summarise the results below.

**Pipe coupling scheme** The coupling design involving the use of dowels to align the pipe ends was problem-free, and allowed the trolley tracks to be aligned to a level of accuracy such that no discernible “bump” was seen in accelerometer measurements when going over the join at tracking speed. Millimetre-sized gaps

between pipes were found to be acceptable, and this means that the squareness requirements of the pipe are substantially reduced compared to a scheme involving flanges.

The vacuum integrity of the test rig demonstrated that there are no substantial problems in achieving a joint which is both flexible (to remove error build-up from pipe to pipe) and acceptably vacuum-tight.

**Pipe supports** The current design incorporating steel flexure legs with cradles for the pipes have been shown to be easy to set up and to allow straightforward installation of the pipes. The finite-element model for the support system was validated and predicts that extrapolation of the pipe and support system to 200m length should pose no particular problems with undamped resonances.

**Carriage trajectory** Direct tests of a trolley with a retro-reflector showed that the samples of pipe purchased “off-the-shelf” met all the straightness requirements consistent with an active shear-control system. The straightness parameter which was most stringent, that for trolley pitch and yaw, still had a 50% margin of safety in the worst case.

The scheme used to measure the pipes showed that optical measurement of the beam shear using a laser is straightforward, and this can serve as a prototype for the sensor in the shear-correction servo.

**Control and communication** The use of off-the-shelf RF communications inside cylindrical conducting pipes was shown to be effective. The risk that there might be nulls in the radiation pattern due to reflections in the pipe which could not be controlled by standard waveguide techniques was demonstrated to be low. The initial RF transmission system was somewhat noisy, but this has now been replaced by a quieter set of modules which show adequate performance.

**Power transmission** A simple inductive power transmission system was shown to be superior in terms of friction performance to conventional dragged-cable solutions, providing adequate power and power stability such that it had no discernible effect on the performance of the COAST trolley when compared with a wired supply. The mechanical effects of the inductive scheme scale to 200m of travel much more favourably than dragged-cable solutions, and extrapolation of the electrical performance to this length of travel was shown to present no serious obstacles.

**Trolley roll** Tests with a trolley with a low centre of gravity show that it was self-correcting with respect to “roll”. Should a higher-centre-of-gravity design be adopted, the tests show that any forces tending to make the trolley roll only have a discernible effect over many trolley lengths of travel, and therefore designing a low-bandwidth servo to achieve adequate stability should present few problems. Simple actuation schemes for such a servo, either by steering one wheel or by shifting a weight, were shown to be feasible and have no discernible impact on the level of trolley vibration and hence pose no risk of additional OPD jitter.

**OPD disturbance tests** The use of compliant wheels was shown to give the expected isolation from vibrations of the pipe and support. More importantly, the use of compliant wheels gave a lower level of trolley vibration when running on the unfinished inner surface of the test rig pipes than seen on the COAST trolley when running on polished steel rails (see Fig. 9). A preliminary model of the disturbance rejection of the MROI cats-eye servo, validated using the COAST trolley, shows that all the OPD stability requirements can be met with more than adequate margins.

**Metrology** Analyses showed that with a suitably expanded metrology laser beam, there is little risk of loss of the metrology signal due to diffraction or alignment drifts, and that even without an active beam shear correction system, the level of beam shear arising from non-straightness of pipes would not cause metrology signal loss. The wavelength stability of a commercial Zygo laser was shown to be adequate for correction over a full 380 m path.

In most cases the results of the experiments met expectations, and any surprises that occurred during the performance of the experiments were almost entirely positive. For example, the test trolley running on compliant wheels on an unfinished pipe surface exhibited generally lower vibrations than the COAST trolley running on polished rails, the trolley turned out to be remarkably resistant to attempts to make it “roll” inside the circular pipe, and little increase in vibration levels was seen when the trolley wheels rolled over gaps of many millimetres between the pipes.

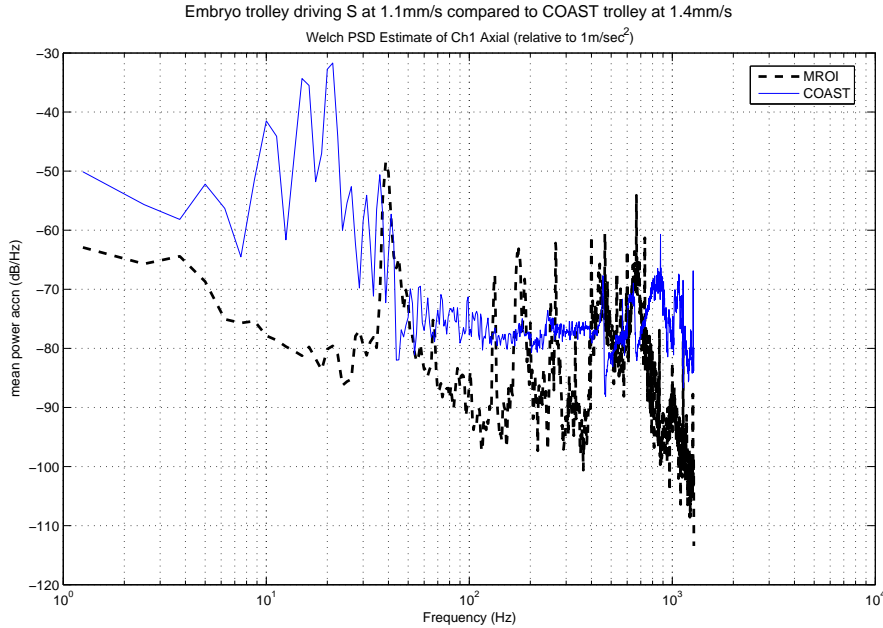


**Figure 9.** Comparison of COAST and embryo trolley axial acceleration power spectra. It can be seen that the embryo trolley running inside the unfinished pipe generally had 10-20dB *less* vibration than the COAST trolley running on polished steel rails. The disturbances seen at high frequencies on the embryo trolley are vibrations due to a poorly tuned drive motor servo. Note also that, because these are *acceleration* spectra, the high frequency vibrations correspond to very small displacements.

## 6. RECENT AND FUTURE PROGRESS

Having validated the major components of our proposed design (including submitting the results of the tests for review by an external panel of experts) we have now embarked on the process of designing and constructing the full-size trolley prototype and a 20-metre-long run of pipes to act as a test rig.

The major mechanical components of the Cat's-eye, including the mirrors, the carbon-fibre main tube and the active secondary support have been manufactured and assembled, and we will begin testing these in June. Many components of the carriage, including the 14-inch diameter aluminium tube which comprises the chassis, the motors, gears and wheels have arrived, and further components are undergoing design and finite-element analysis (FEA). The architecture of the software has been defined and device drivers are being written. In common with many modern technical projects, much of the functionality has been devolved onto software, and it is the software coding and test which on the critical path for the completion of the prototype.

After extensive testing of the prototype towards the end of 2006, the design will be reworked based on the results of these tests before a Final Design Review in early 2007. It is intended to deliver the first production trolley to NMT mid 2007. NMT are responsible for procuring the pipes and supports for six 190-m long delay lines and installing them in the 200-m long Delay Line Area of the MROI Beam Combining Facility (BCF). The drawing package for the BCF has been sent to the pre-qualified building contractors in May and the buildings are due to be completed in August 2007.

## 7. CONCLUSIONS

Traditional systems for path compensation for long-baseline interferometers are multi-stage designs, which compromise faint-source science. We are prototyping a delay line capable of introducing 0-380 metres of optical delay in a single stage. The advantages of having all the delay in a single stage include:

1. Fewer reflections and therefore higher interferometric SNR.
2. Fewer subsystems to operate and maintain. In addition we have demonstrated the use of contactless power transmission and communication inside the vacuum pipes, which should further increase system reliability.
3. Interferometric access to any star above 30° elevation within 5 minutes, and without requiring realignment.
4. Simpler and more reliable baseline modelling from small numbers of delay measurements.

The innovative aspects of our design were tested in a series of experiments and the results were, if anything, better than expected. We expect to deliver the delay lines to MROI well in advance of the target date for MROI “first fringes” in 2008.

## 8. ACKNOWLEDGEMENTS

We thank Mark Colavita, Dennis Coyne, Sergio Restaino, Mark Swain and Wes Traub for their commitment of time and their helpful comments at the the delay line reviews.

Magdalena Ridge Observatory (MRO) is funded by Agreement No. N00173-01-2-C902 with the Naval Research Laboratory (NRL). The MRO Interferometer is hosted by New Mexico Institute of Mining and Technology (NMT) at Socorro, NM, USA, in collaboration with the University of Cambridge (UK).

## REFERENCES

1. J. S. Young and D. F. Buscher, “Telescope primary mirror size,” Interferometer Working Group Memo INT-402-MIS-0005, Magdalena Ridge Observatory, 2003.
2. P. B. Gitton, M. Cantzler, B. Koehler, and P. Kervella, “VLTI image alignment monitoring,” in *Interferometry for Optical Astronomy II. Edited by Wesley A. Traub . Proceedings of the SPIE, Volume 4838, pp. 1182-1192 (2003).*, W. A. Traub, ed., pp. 1182–1192, Feb. 2003.
3. M. A. Hrynevych, K. Tsubota, R. F. Smythe, W. Dahl, J. Bell, M. M. Colavita, J. Gathright, F. Meggars, C. R. Neyman, A. C. Rudeen, G. T. van Belle, and P. L. Wizinowich, “Keck Interferometer autoaligner: algorithms and techniques,” in *New Frontiers in Stellar Interferometry, Proceedings of SPIE Volume 5491. Edited by Wesley A. Traub. Bellingham, WA: The International Society for Optical Engineering, 2004., p.1061*, W. A. Traub, ed., pp. 1061–+, Oct. 2004.
4. J. H. Clark, L. Ha, D. Mozurkewich, and J. T. Armstrong, “Design of the long delay lines for the Navy Prototype Optical Interferometer,” in *Proc. SPIE Vol. 3350, p. 497-504, Astronomical Interferometry, Robert D. Reasenberg; Ed., R. D. Reasenberg, ed., pp. 497–504, July 1998.*
5. J. E. Baldwin, M. G. Beckett, R. C. Boysen, D. Burns, D. F. Buscher, G. C. Cox, C. A. Haniff, C. D. Mackay, N. S. Nightingale, J. Rogers, P. Scheuer, T. R. Scott, P. G. Tuthill, P. J. Warner, D. M. A. Wilson, and R. W. Wilson, “The first images from an optical aperture synthesis array - mapping of Capella with COAST at 2 epochs,” *Astron. Astrophys.* **306**, pp. L13–L16, 1996.